The Movement-Rotation (MR) Correlation Function and Coherence Distance of VLC Channels

Jiaxuan Chen, Iman Tavakkolnia, Cheng Chen, Zhaocheng Wang and Harald Haas

***Abstract*—Adaptive transmission based on instantaneous channel state information is an important methodology to improve data rates of mobile users, which requires the periodic update of channel variations. Different from radio frequency (RF) channels, whose variations are governed by Doppler and multi-path effects, visible light communication (VLC) channel variations are mainly related to receiver movements and rotations. In this paper, a movement-rotation (MR) correlation function is proposed to measure VLC channel variations with the changes in receiver location and orientation. The correlation function of VLC channel gain in the time domain can then be approximated by the MR correlation function, which is an important criterion for the design of data transmission frames. It is verified that the approximation by MR correlation function can approach the actual simulation and experiment results of VLC channel gain correlation function in the time domain. In addition, experiment and simulation results are presented to investigate variation characteristics of VLC channels in different scenarios. It is shown that a receiver movement of several decimeters or a change of 10-20 degrees in the inclined angle of the receiver is required in a typical scenario in order to observe a distinguishable change of VLC channel gain.**

***Index Terms*—Visible light communications channels, correlation function, channel variations**

I. Introduction

With the increasing deployment of mobile devices, data traffic in wireless communication networks has grown tremendously in recent years, which requires the use of new spectrum in addition to the existing radio frequency (RF) spectrum. Visible light communications (VLC) is a promising candidate which uses unlicensed spectrum, is energy efficient and can harness high spatial reuse gains [1], [2]. In VLC networks, light sources, such as light-emitting-diodes (LED), are utilized as data transmitters and photodiodes (PDs) serve as receivers. Due to the much shorter wavelength of visible light compared with the size of PDs, VLC channels can be modeled by geometrical optics and are usually dominated by line-of-sight paths [2], [3]. Therefore, if the receiver location and orientation is fixed compared with the transmitter, the VLC channel is quasi-static. In other words, variations of the VLC channel for a receiver are mainly incurred by the receiver's movements and rotations, which is different from conventional RF channels [4]. Therefore, the distinctive features of the VLC channel should be investigated.

The characteristics of the instantaneous VLC channel impulse response assuming fixed LED and PD locations have been well studied. For instance, the spectral response and the transmission bandwidth of the VLC channel impulse response were studied in [3]–[7]. However, in mobile scenarios, due to the randomness of the receiver orientation and location, VLC channel gains are actually variable. The probability density function of VLC channel gains under random receiver location and orientation was introduced in [8], which shows that VLC channel gains at different receiver locations and orientations could be very different. Therefore, it is beneficial to adapt transmission schemes periodically based on the instantaneous channel state information (CSI). In [9], [10], it is demonstrated that adaptive transmission schemes using instantaneous CSI are able to improve system throughput greatly. However, in order to obtain those performance gains, the frequency of CSI updates should be at least similar to the pace of channel variations to guarantee the accuracy of CSI. Therefore, the investigation into the dynamic changes of the VLC channel for mobile receivers is crucial to the design and analysis of adaptive data transmission, such as deciding when and where to feedback CSI. In [8], [11], the variation of receiver orientation over time was investigated, which underpins the study of VLC channel variations caused by receiver rotation. Channel variations and sojourn time for LiFi cellular networks under receiver movements were studied in [12], [13]. However, there is not yet a general metric to specify the dynamic changes of VLC channel gain due to the joint effect of receiver movements and rotations. To avoid any confusion, the receiver movement only refers to the change in receiver location, while the change in receiver orientation is referred to as receiver rotation.

The correlation function of channel gain in the time domain and coherence time are commonly used to quantify channel variation characteristics [14]–[16]. For conventional RF channels, the correlation function in the time domain is determined by the Doppler effect [14]. However, in VLC systems, since intensity modulation/direct detection (IM/DD) scheme is adopted and there is no high-frequency carrier, Doppler effect is marginal. Hence, the equations about correlation function of channel gain in the time domain and coherence time derived for RF channels can not be applied. Instead, the correlation function of VLC channel gain in the time domain should be derived by jointly considering the receiver

J. Chen and Z. Wang are with Beijing National Research Center for Information Science and Technology (BNRist), Department of Electronic Engineering, Tsinghua University, Beijing 100084, China, and Z. Wang is also with Division of Information Science and Technology, Graduate School at Shenzhen, Tsinghua University, Shenzhen 518055, China (E-mails: chenjx16@mails.tsinghua.edu.cn, zcwang@tsinghua.edu.cn).

I. Tavakkolnia, C. Chen and H. Haas are with the LiFi Research and Development Centre, Institute for Digital Communications, The University of Edinburgh, Edinburgh EH9 3JL,U.K (E-mails: I. Tavakkolnia@ed.ac.uk, Cheng.Chen@ed.ac.uk, h.haas@ed.ac.uk).

This work was supported in part by National Natural Science Foundation of China (Grant No. 61871253). H. Haas acknowledges the financial support from the Wolfson Foundation and Royal Society. He also gratefully acknowledges financial support by the Engineering and Physical Sciences Research Council (EPSRC) under the Established Career Fellowship grants EP/R007101/1and EP/S016570/1 'Terabit Bidirectional Multi-User Optical Wireless System (TOWS) for 6G LiFi'.*(Corresponding author: Zhaocheng Wang)*

movement and rotation characteristics. Nevertheless, since the correlation function of VLC channel gain in the time domain only has one variable, namely time, the effects of receiver movement and rotation are coupled and can not be evaluated separately. Therefore, a novel correlation function is defined to measure VLC channel variations due to receiver movement and rotation directly and without time dependence, referred to as the movement-rotation (MR) correlation function. The main contributions of our work are listed below

- Using the general definition of correlation function, the MR correlation function is proposed to indicate the dependencies or variations of VLC channel gains as a function of receiver movement and rotation. Accordingly, coherence distance is defined to offer a range of receiver movement and rotation, within which VLC channels stay relatively stable.
- An approximation of the correlation function of VLC channel gain in the time domain, as well as coherence time, is proposed based on the MR correlation function, given statistical information about receiver movements and rotations over time.
- Applications of the MR correlation function in system design are investigated. In particular, the relationship between CSI feedback frequency and the fluctuations of the achievable spectral efficiency is studied using the MR correlation function, which facilitates improving the efficiency of CSI feedback.

The MR correlation function specifies the features of VLC channel changes due to receiver movements and rotations. According to our experiment and simulation results in various scenarios, a receiver should move several tens of centimeters or its inclination angle should change 10-20 degrees, in order to have a distinct channel gain alteration, or more specifically, to decrease the channel correlation below 90%. At the same time, utilizing the statistical information of receiver behavior, such as its velocity, the VLC channel variations as a function of receiver movement and rotation can be transferred to the channel variations in the time domain, which can then be used to determine the frequency of CSI update.

The rest of the paper is organized as follows. In Section II, the definitions and calculations of the MR correlation function and coherence distance are introduced. In Section III, experiment and simulation results of the MR correlation function and coherence distance in an actual VLC system are illustrated, based on which the features of VLC channel variations in this VLC system is specified. The features of VLC channel variations in different scenarios are then compared in Section IV. In Section V, the MR correlation function is utilized to approximate the correlation function of VLC channel gain in the time domain. In Section VI, the MR correlation function is applied to the analysis of system performances under varying VLC channels. Finally, conclusions and future works are drawn in Section VII.

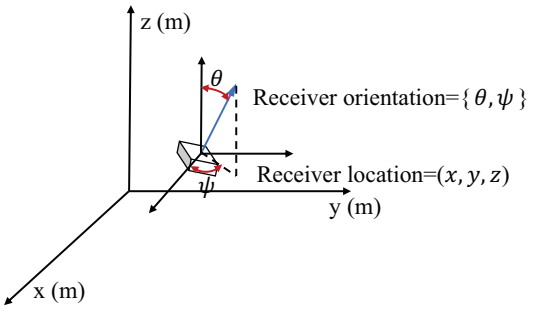

Fig. 1. A diagram of receiver state including the receiver location $\boldsymbol{R}$ and receiver orientation $\{\theta, \psi\}$.

II. MR Correlation Function in VLC Systems

A. Definition of the MR correlation function

A point-to-point VLC system is considered, where one LED serves one user that is equipped with one PD receiver. The VLC channel gain between the receiver and the LED is denoted as $h(\boldsymbol{R}, \theta, \psi)$, where $\boldsymbol{R}$ denotes the receiver's three-dimensional location and $\{\theta, \psi\}$ represent its orientation. Specifically, θ is the polar angle of the normal vector for the receiver, while ψ denotes the azimuthal angle, as shown in Fig. 1. Without loss of generality, receiver location is defined in a Cartesian coordinate system with the LED as the origin point. The set including the receiver's location and orientation is referred to as a receiver state and is denoted as $\{\boldsymbol{R}, \theta, \psi\}$.

In order to measure channel variations in the VLC system, the MR correlation function of VLC channel gain over receiver movement $\Delta r\boldsymbol{n}$ and rotation $\{\Delta\theta, \Delta\psi\}$ is defined as,

$$\begin{aligned} &C(\Delta r\boldsymbol{n}, \Delta\theta, \Delta\psi) \qquad (1)\\ &= E\{(h(\boldsymbol{R}, \theta, \psi) - \bar{h})(h(\boldsymbol{R} + \Delta r\boldsymbol{n}, \theta + \Delta\theta, \psi + \Delta\psi) - \bar{h})\}\\ &= \iiint (h(\boldsymbol{R}, \theta, \psi) - \bar{h})(h(\boldsymbol{R} + \Delta r\boldsymbol{n}, \theta + \Delta\theta, \psi + \Delta\psi) - \bar{h})\\ &\qquad \times f(\boldsymbol{R}, \theta, \psi | \Delta r\boldsymbol{n}, \Delta\theta, \Delta\psi)\, d\boldsymbol{R}\, d\theta\, d\psi \end{aligned}$$

where $\boldsymbol{n}$ is a normalized vector representing the direction of receiver movement and Δr denotes the movement at the direction $\boldsymbol{n}$. $\Delta\theta$ and $\Delta\psi$ denote the changes of polar angle and azimuthal angle respectively. $f(\boldsymbol{R}, \theta, \psi | \Delta r\boldsymbol{n}, \Delta\theta, \Delta\psi)$ is the joint probability density function (PDF) of the receiver location and orientation conditioned on receiver movement and rotation $\Delta r\boldsymbol{n}, \Delta\theta, \Delta\psi$. $\bar{h}$ is the average channel gain from the LED to the receiver, calculated as

$$\bar{h} = \iiint h(\boldsymbol{R}, \theta, \psi) f(\boldsymbol{R}, \theta, \psi)\, d\boldsymbol{R}\, d\theta\, d\psi \qquad (2)$$

where $f(\boldsymbol{R}, \theta, \psi)$ denotes the PDF of receiver state $\{\boldsymbol{R}, \theta, \psi\}$. Moreover, to provide a fair measurement of VLC channel variations in different scenarios, the MR correlation function is normalized as

$$\rho(\Delta r\boldsymbol{n}, \Delta\theta, \Delta\psi) = \frac{C(\Delta r\boldsymbol{n}, \Delta\theta, \Delta\psi)}{C(0, 0, 0)} \qquad (3)$$

Invoking the definition of coherence time in [15], we can further define the coherence distance as follows, which describes the normalized MR correlation in an inverse point of view.

Definition 1. *Given the change of receiver orientation as* $\{\Delta\theta, \Delta\psi\}$*, coherence distance* $d(\boldsymbol{n}, \Delta\theta, \Delta\psi, \alpha)$ *is defined as the minimum movement* r *in the direction* $\boldsymbol{n}$*, such that the normalized MR correlation function is smaller than a threshold* α*, i.e.,*

$$d(\boldsymbol{n}, \Delta\theta, \Delta\psi, \alpha) = \min\{r \in R^+ | \rho(r\boldsymbol{n}, \Delta\theta, \Delta\psi) \leq \alpha\} \quad (4)$$

Generally, the coherence distance provides a boundary of receiver movements and rotations, within which the VLC channel gains are relatively similar. The threshold α specifies the similarity of VLC channel gains within the coherence distance. For example, $\alpha = 0.9$ indicates that the correlation of VLC channel gains during a movement in the direction $\boldsymbol{n}$ is higher than 90% if the receiver movement is shorter than the coherence distance $d(\boldsymbol{n}, \Delta\theta, \Delta\psi, 0.9)$ and the change of receiver orientation is limited by $\{\Delta\theta, \Delta\psi\}$. Whereas, $\alpha = 0$ means that the VLC channel gain could become entirely uncorrelated after a receiver movement of $d(\boldsymbol{n}, \Delta\theta, \Delta\psi, 0)$ and a receiver rotation of $\{\Delta\theta, \Delta\psi\}$.

We can also get the average coherence distance over all movement directions, which is denoted as $\bar{d}(\Delta\theta, \Delta\psi, \alpha)$ and formulated as

$$\bar{d}(\Delta\theta, \Delta\psi, \alpha) = \min\{r \in R^+ | E_{\boldsymbol{n}}\{\rho(r\boldsymbol{n}, \Delta\theta, \Delta\psi)\} \leq \alpha\} \quad (5)$$

For most mobile users on the ground, the vertical changes in the receiver location are limited, compared with the horizontal receiver movements [11]. In this work, only receiver movements in a horizontal user plane are considered, namely that Δz is assumed to be zero. Fig. 2 depicts the difference between coherence distance and average coherence distance. For the receiver marked by the red cross, the coherence distance in different receiver movement directions could be different, when the VLC channel gain or the conditional PDF of receiver location and orientation is not symmetrical. On the contrary, by averaging all movement directions, the average coherence distance $\bar{d}(\Delta\theta, \Delta\psi, \alpha)$ gives an isotropic boundary of the receiver movement. Specifically, if receiver rotation is limited by $\{\Delta\theta, \Delta\psi\}$ and the receiver moves a distance shorter than $\bar{d}(\Delta\theta, \Delta\psi, \alpha)$ at any direction $\boldsymbol{n}$, the correlation of VLC channel gains during the movement is, on average, higher than α.

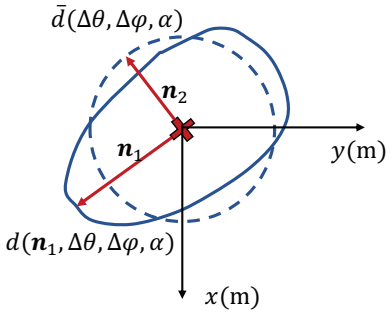

Fig. 2. Illustration of coherence distance and average coherence distance.

B. Calculation of the MR correlation function

The calculation of the MR correlation function is performed by a central controller at the transmitter side, which requires channel gains $h(\boldsymbol{R}, \theta, \psi)$ and the conditional PDF $f(\boldsymbol{R}, \theta, \psi | \Delta r\boldsymbol{n}, \Delta\theta, \Delta\psi)$ according to (1). The channel gains at different receiver states could be sampled by the user and fed back via its uplink. Interpolation techniques can then be used at the central controller to get channel gains at any receiver state. The conditional PDF $f(\boldsymbol{R}, \theta, \psi | \Delta r\boldsymbol{n}, \Delta\theta, \Delta\psi)$ can be rewritten as

$$f(\boldsymbol{R}, \theta, \psi | \Delta r\boldsymbol{n}, \Delta\theta, \Delta\psi) = \frac{f(\boldsymbol{R}, \theta, \psi, \Delta r\boldsymbol{n}, \Delta\theta, \Delta\psi)}{f(\Delta r\boldsymbol{n}, \Delta\theta, \Delta\psi)} \quad (6)$$

where $f(\boldsymbol{R}, \theta, \psi, \Delta r\boldsymbol{n}, \Delta\theta, \Delta\psi)$ denotes the PDF that a receiver movement and rotation $\Delta r\boldsymbol{n}, \Delta\theta, \Delta\psi$ from receiver state $\{\boldsymbol{R}, \theta, \psi\}$ occurs at a user trajectory. $f(\Delta r\boldsymbol{n}, \Delta\theta, \Delta\psi)$ is the joint PDF of receiver movement and rotation, which can be calculated after $f(\boldsymbol{R}, \theta, \psi, \Delta r\boldsymbol{n}, \Delta\theta, \Delta\psi)$. Similar to the methods in [17], the PDF $f(\boldsymbol{R}, \theta, \psi, \Delta r\boldsymbol{n}, \Delta\theta, \Delta\psi)$ is approximated by its discrete version based on collected user trajectories.

Firstly, the possible values of the multivariable group including receiver state, receiver movement and rotation, denoted as $\{\boldsymbol{R}, \theta, \psi, \Delta r\boldsymbol{n}, \Delta\theta, \Delta\psi\}$, is quantized. Assuming the center of a quantized region is $\{\boldsymbol{R}_c, \theta_c, \psi_c, \Delta\boldsymbol{r}_c, \Delta\theta_c, \Delta\psi_c\}$, the quantized region is formulated as

$$\Big\{\{\boldsymbol{R}, \theta, \psi, \Delta\boldsymbol{r}, \Delta\theta, \Delta\psi\} : \boldsymbol{R}_c - \epsilon_1 \leq \boldsymbol{R} \leq \boldsymbol{R}_c + \epsilon_1, \quad (7)$$
$$\theta_c - \epsilon_2 \leq \theta \leq \theta_c + \epsilon_2, \psi_c - \epsilon_3 \leq \psi \leq \psi_c + \epsilon_3,$$
$$\Delta\boldsymbol{r}_c - \epsilon_1 \leq \Delta\boldsymbol{r} \leq \Delta\boldsymbol{r}_c + \epsilon_1, \Delta\theta_c - \epsilon_2 \leq \Delta\theta \leq \Delta\theta_c + \epsilon_2,$$
$$\Delta\psi_c - \epsilon_3 \leq \Delta\psi \leq \Delta\psi_c + \epsilon_3\Big\}$$

where $\epsilon_i, i = 1, 2, 3$ determines the size of the quantized region. A user trajectory is a path for receiver states, which represents the changes in receiver state over time and can be denoted as $\{\boldsymbol{R}_t, \theta_t, \psi_t\}$. $\boldsymbol{R}_t$ is the receiver location at time t and $\{\theta_t, \psi_t\}$ denotes the receiver orientation at time t. After quantization, the user trajectory can then be represented by a set of quantized regions of receiver state, denoted as $\{\{\boldsymbol{R}_k, \theta_k, \psi_k\} : 1 \leq k \leq N\}$. $\{\boldsymbol{R}_k, \theta_k, \psi_k\}$ is the center of the k-th quantized region of receiver state that the user trajectory passes through and N represents the number of all quantized regions of receiver state on the user trajectory.

As a result, on the quantized user trajectory, each event of receiver movement and rotation from a receiver state corresponds to a pair $\{t_1, t_2 : 1 \leq t_1, t_2 \leq N\}$. Specifically, the event related to the pair $\{t_1, t_2\}$ means the receiver movement and rotation $\{\boldsymbol{R}_{t_2} - \boldsymbol{R}_{t_1}, \theta_{t_2} - \theta_{t_1}, \psi_{t_2} - \psi_{t_1}\}$ from receiver state $\{\boldsymbol{R}_{t_1}, \theta_{t_1}, \psi_{t_1}\}$, which is denoted by the multivariable group $\{\boldsymbol{R}_{t_1}, \theta_{t_1}, \psi_{t_1}, \boldsymbol{R}_{t_2} - \boldsymbol{R}_{t_1}, \theta_{t_2} - \theta_{t_1}, \psi_{t_2} - \psi_{t_1}\}$.

Therefore, the probability of the multivariable group $\{\boldsymbol{R}, \theta, \psi, \Delta r\boldsymbol{n}, \Delta\theta, \Delta\psi\}$ landing in one quantized region can be calculated as the number of events related to the specific quantized region divided by the number of all events. More specifically, we have

$$f(\boldsymbol{R}, \theta, \psi, \Delta r\boldsymbol{n}, \Delta\theta, \Delta\psi)\mathrm{d}\boldsymbol{R}\mathrm{d}\theta\mathrm{d}\psi\mathrm{d}\Delta r\boldsymbol{n}\mathrm{d}\Delta\theta\mathrm{d}\Delta\psi = \frac{\mathcal{A}(\boldsymbol{R}, \theta, \psi, \Delta r\boldsymbol{n}, \Delta\theta, \Delta\psi)}{\mathcal{B}} \quad (8)$$

where $\mathcal{A}(\boldsymbol{R}, \theta, \psi, \Delta r\boldsymbol{n}, \Delta\theta, \Delta\psi)$ means the number of events on the collected user trajectories whose corresponding multivariable group lies in the same quantized region as $\{\boldsymbol{R}, \theta, \psi, \Delta r\boldsymbol{n}, \Delta\theta, \Delta\psi\}$. $\mathcal{B}$ denotes the number of all events. Large number of events should be considered to improve the approximation accuracy of (8), which can be achieved by utilizing more number of user trajectories. Afterwards, $f(\boldsymbol{R}, \theta, \psi)$ and $f(\boldsymbol{R}, \theta, \psi|\Delta r\boldsymbol{n}, \Delta\theta, \Delta\psi)$ can be calculated according to $f(\boldsymbol{R}, \theta, \psi, \Delta r\boldsymbol{n}, \Delta\theta, \Delta\psi)$.

It is worth noting that it is not necessary to collect channel gains and user trajectories simultaneously. To ensure the accuracy of $f(\boldsymbol{R}, \theta, \psi, \Delta r\boldsymbol{n}, \Delta\theta, \Delta\psi)$, multiple user trajectories should be used. Each quantized region of the receiver state might belong to several trajectories. However, it is redundant to collect and store the channel gain in a certain quantized region of the receiver state multiple times when different user trajectories pass it, because the channel gain at a certain receiver state is quasi-static. When the receiver movement pattern changes, we only have to update the database of user trajectories. There is no need to collect VLC channel gains at different receiver states again. Therefore, it can be an efficient way to process and store the channel gains $h(\boldsymbol{R}, \theta, \psi)$ and joint PDF $f(\boldsymbol{R}, \theta, \psi, \Delta r\boldsymbol{n}, \Delta\theta, \Delta\psi)$ separately.

III. The Illustration of MR Correlation Function in a Typical VLC System

In this section, the MR correlation function of the VLC channel gain in an empty room is illustrated. According to (1), the calculation of the MR correlation function needs the VLC channel gain at different receiver states, $h(\boldsymbol{R}, \theta, \psi)$, as well as the conditional PDF of receiver location and orientation, $f(\boldsymbol{R}, \theta, \psi|\Delta\boldsymbol{r}, \Delta\theta, \psi)$. Firstly, we conducted an experiment to measure the VLC channel gains in a 2.6 m $\times$ 2.6 m room, where a lamp is deployed at the center of the ceiling for data transmission and is 2.31 meters above the floor. According to the instruction manual of the lamp used in the manuscript, its semi-angle at half illuminance, denoted as $\Phi_{1/2}$, is 33°. An LED light meter is utilized to test channel gains on the floor and its field-of-view (FOV), denoted as Φ_c, is 80°.

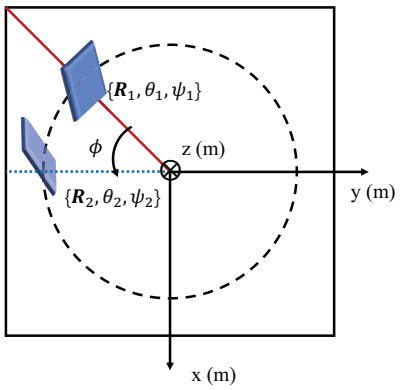

Fig. 3. The experiment setup.

In the experiment, the channel gains on the 1.8 m line segment from the center of the floor to the corner were tested, as illustrated by the red line segment in Fig. 3. The spacing between two adjacent testing points is 0.1 m. At each testing point on the line segment, the channel gains, having ψ sampled from 0 to 360° with an interval of 90°, and θ sampled from 0 to 90° with an interval of 10°, are tested. Afterwards, linear interpolation is utilized to obtain the channel gain at any receiver state on the line segment.

Since the illuminance of the lamp is symmetrical in terms of the receiver state, the VLC channel gains at other points on the floor can be acquired by the tested channel gains on that line segment. Specifically, any receiver state $\{\boldsymbol{R}_2, \theta_2, \psi_2\}$ on the floor can be obtained by rotating a receiver state $\{\boldsymbol{R}_1, \theta_1, \psi_1\}$ on the red line around the z-axis by an angle ϕ. As shown in Fig. 3, there exist $\boldsymbol{R}_1$ and ϕ, such that $\boldsymbol{R}_2 = \boldsymbol{T}(\phi)\boldsymbol{R}_1$, $\psi_2 = \psi_1 + \phi$ and $\theta_2 = \theta_1$, where $\boldsymbol{T}(\phi)$ is the rotation matrix about z-axis by an angle ϕ. Due to the symmetrical illuminance of the lamp, we have $h(\boldsymbol{R}_2, \theta_2, \psi_2) = h(\boldsymbol{R}_1, \theta_1, \psi_1)$.

Figure 4 shows the tested VLC channel gain divided by its maximum value, when $\theta = 0^\circ$. It can be seen that the VLC channel gain in the room is symmetrical in terms of the receiver location and can reach the peak value at the center of the room when the receiver orientation is upward. When the receiver orientation is not vertical, the VLC channel gain is not a symmetrical function over the receiver location anymore and the peak of the VLC channel gain curve will shift from the center, as shown in Fig. 5

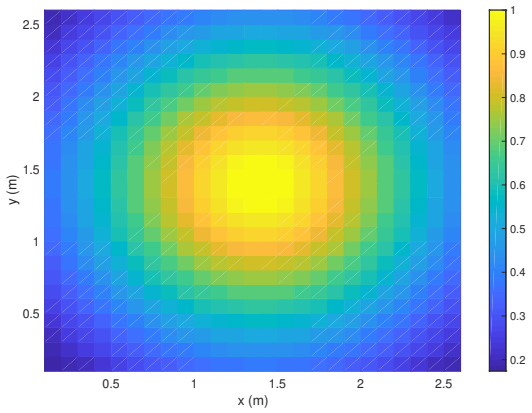

Fig. 4. The experimental VLC channel gains when $\theta = 0^\circ$.

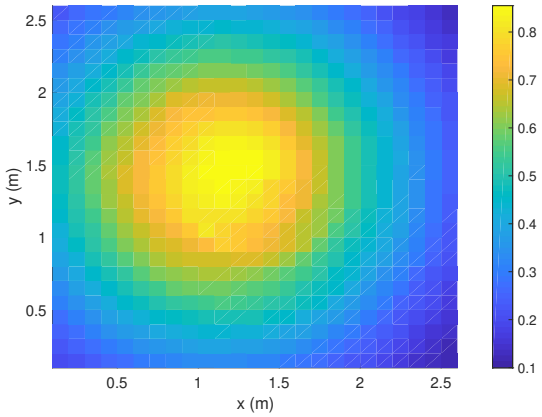

Fig. 5. The experimental VLC channel gains when $\theta = 40^\circ, \psi = 0^\circ$.

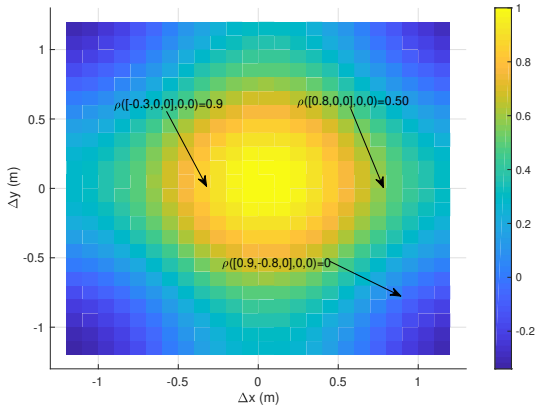

Fig. 6. The normalized MR correlation function of the experimental VLC channel gains with $\Delta\theta = 0^\circ$ and $\Delta\psi = 0^\circ$.

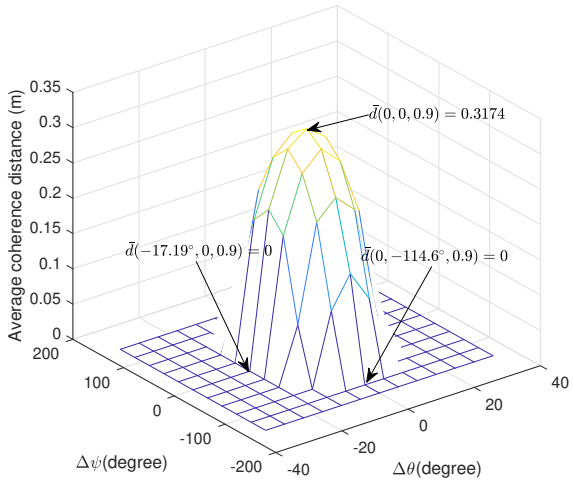

Fig. 7. The average coherence distance of the experimental VLC channel gains with $\alpha = 0.9$.

To compute the MR correlation function, the conditional PDF of receiver location and orientation, i.e. $f(\boldsymbol{R}, \theta, \psi | \Delta r \boldsymbol{n}, \Delta\theta, \Delta\psi)$, is required, besides the VLC channel gain $h(\boldsymbol{R}, \theta, \psi)$. [8], [11] have conducted experiments to study user trajectories, based on which the authors proposed a user mobility model. Instead of repeating the experiments in [8], [11], we directly adopt the orientation-based random waypoint (ORWP) mobility model in [8] to simulate user trajectories in this work, where the polar angle θ obeys the truncated Gaussian distribution with a mean of 28° and a standard deviation of 7.8°. Then, the conditional PDF of receiver location and orientation is computed as in (8). 5000 user trajectories, including more than 1.5×10^5 receiver states in the discrete formulation of these user trajectories, are utilized, in order to realize a tradeoff between the accuracy and computational complexity. Given the conditional PDF of receiver location and orientation $f(\boldsymbol{R}, \theta, \psi | \Delta r \boldsymbol{n}, \Delta\theta, \Delta\psi)$ and the experimental VLC channel gain $h(\boldsymbol{R}, \theta, \psi)$, the MR correlation function of the experimental VLC channel gain can be calculated by (1). Fig. 6 shows the normalized MR correlation function of the experimental VLC channel gain when $\Delta\theta$ and $\Delta\psi$ are both 0. For example, the normalized MR correlation function $\rho(\Delta r \boldsymbol{n}, 0, 0) \simeq 0.9$ when Δr is about 0.3 m, while when Δr is around 1.2 m, the normalized MR correlation function approximately drops to 0. According to the curves of the VLC channel gain in Figs. 4 and 5, a movement of 0.3 m yields fairly small channel variations. However, after a movement of 1.2 m, the VLC channel gain could become completely different. For instance, a user could step from the dark area to the bright area or to the opposite dark area by moving 1.2 m. Therefore, to avoid apparent channel changes, receiver movement should be bounded by the coherence distance or average coherence distance with a high threshold α.

Since the MR correlation function is a multivariable function, it is difficult to get an explicit impression on the effects of all its parameters directly. Coherence distance and average coherence distance, namely $d(\boldsymbol{n}, \Delta\theta, \Delta\psi, \alpha)$ and $\bar{d}(\Delta\theta, \Delta\psi, \alpha)$, are easier ways to describe the effects of receiver movement and rotation visually. Fig. 7 shows the average coherence distance of the experimental VLC channel gain with $\alpha = 0.9$, based on the MR correlation function. In general, when $\Delta\theta, \Delta\psi$ equal to 0, the average coherence distance with threshold $\alpha = 0.9$ is around 0.3 m, which means the channel gain at a position is in average 90% correlated with the channel gain 0.3 m away. However, if the receiver rotation is non-negligible, the average coherence distance will be decreased. When $\Delta\theta$ is around 17 degrees, the average coherence distance is nearly zero, which means that the correlation between VLC channel gains will drop lower than 0.9 after θ changing 17 degrees regardless of receiver movement. In addition, the average coherence distance is nearly zero if $\Delta\psi \geq 114$ degrees. Therefore, the alteration of the azimuthal angle ψ should be less than 114 degrees to keep the VLC channel relatively static. This also indicates that VLC channel gains are more sensitive to the alteration of polar angle θ than azimuthal angle ψ.

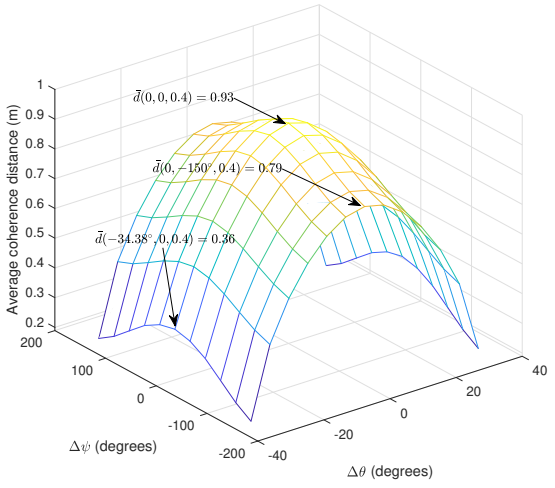

Fig. 8. The average coherence distance of the experimental VLC channel gains with $\alpha = 0.4$.

Figure 8 illustrates the average coherence distance of the experimental VLC channel gain with $\alpha = 0.4$. It can be seen that the impact of receiver rotation on average coherence distance with $\alpha = 0.4$ is reduced in comparison to that with $\alpha = 0.9$. For instance, in Fig. 8, the average coherence distance decreases only slightly with the increase of $\Delta\psi$. Therefore, although receiver rotations could affect VLC channel stability greatly, it is difficult to get nearly uncorrelated channel gains only via receiver rotations. In other words, receiver rotations usually lead to small channel fluctuations, while receiver movements result in large scale channel variations.

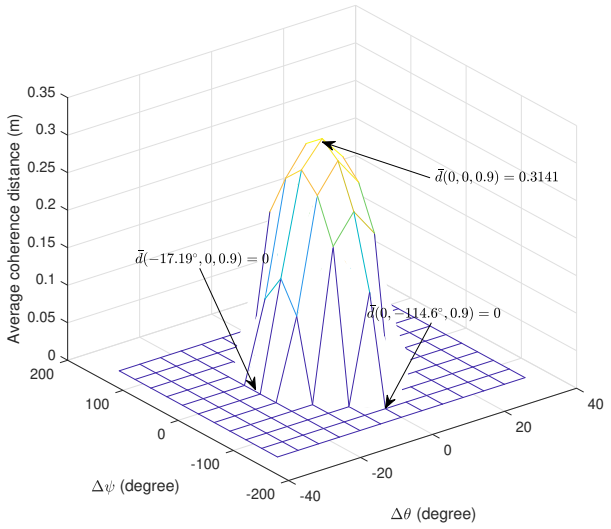

Fig. 9. The average coherence distance of the simulated VLC channel gains with $\alpha = 0.9$.

Moreover, we simulate VLC channel gains according to the general VLC channel model in [4], using the same parameters as the lamp and receiver in the experiments. Accordingly, the MR correlation function of the simulated channel gains is calculated, using the same conditional PDF of receiver location and orientation as in Fig. 7. Fig. 9 shows the average coherence distance of the simulated VLC channel gain with $\alpha = 0.9$, which matches well with the coherence distance of the experimental VLC channel gain in Fig. 7. Therefore, a credible estimation of the MR correlation function and coherence distance can be provided using the general simulation model of VLC channel gains. In the following sections, the VLC channel gains in other VLC systems are computed via simulations.

IV. Important Factors in VLC Channel Variations

The coherence distance and average coherence distance vary with the statistical characteristics of user trajectories, as well as the placement of LEDs. Therefore, in this section, coherence distance and average coherence distance under different types of user trajectories and LED deployments are analyzed.

Considering a 6 m $\times$ 6 m room, an LED is deployed at the center of the ceiling with a height of 2.31 m. As shown in Fig. 10, several cases of user trajectories are considered, in order to investigate VLC channel variations with different user movement ranges and different user movement directions.

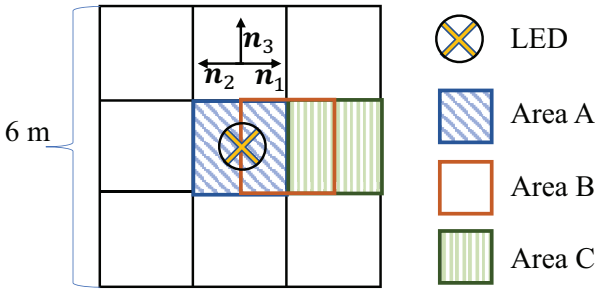

Fig. 10. Illustration of LED deployment and user movement.

Case 1) Moving in area B with direction $\boldsymbol{n}_1$ (away from the LED)

Case 2) Moving in area B with direction $\boldsymbol{n}_2$ (toward the LED)

Case 3) Moving in area B with direction $\boldsymbol{n}_3$

Case 4) Moving in area C with direction $\boldsymbol{n}_1$ (away from the LED)

Case 5) Moving in area C with direction $\boldsymbol{n}_2$ (toward the LED)

Case 6) Moving in area C with direction $\boldsymbol{n}_3$

Case 7) Moving around in the center area A

Case 8) Moving around in the whole 6 m $\times$ 6 m area

Receiver location is assumed to be equal to user location. For Case 7 and 8, user trajectories are simulated using the ORWP mobility model in [8]. For Cases 1-6, user trajectories satisfying the specific movement range and direction are selected from those for Case 7 and 8. In the ORWP mobility model, two modes for the polar angle θ are considered. In mode 1, θ obeys a truncated Gaussian distribution with a mean of $\theta_0 = 28°$ and a standard deviation of $\sigma = 7.8°$, which relates to the scenario where users walk with receivers (their cell phones) in front of them [11]. In mode 2, θ obeys a truncated Gaussian distribution with a mean of $\theta_0 = 0°$ and a standard deviation of $\sigma = 7.8°$, in order to model the orientation of receivers deployed at the top of automatic machines, like robot vacuum cleaners. In addition, the azimuthal angle of the receiver is assumed to be opposite to the azimuthal angle of the user moving direction, namely $\psi = \Phi + \pi$, where Φ denotes the azimuthal angle of user movement direction $\boldsymbol{n}$. This is because users usually hold their phones in front of them, with the screen facing them [11]. Given the simulated user trajectories, the conditional PDF of receiver location and orientation can be computed as in (8). In addition, the channel gains at different receiver states are calculated according to the channel model in [4]. As a result, the MR correlation function, coherence distance and average coherence distance can be calculated by (1), (4) and (5), respectively.

To illustrate the effects of receiver movement and rotation, there are three key points on the coherence distance or average coherence distance curve, such as the three points marked in Fig. 7. They are 1) (average) coherence distance when the receiver orientation is fixed, i.e. $d(\boldsymbol{n}, 0, 0, \alpha)$ and $\bar{d}(0, 0, \alpha)$; 2) the minimum value of $\Delta\theta$ that satisfies $d(\boldsymbol{n}, \Delta\theta, 0, \alpha) = 0$ or $\bar{d}(\Delta\theta, 0, \alpha) = 0$, referred to as coherence polar angle and

TABLE I
COHERENCE DISTANCE AND COHERENCE POLAR ANGLE FOR CASES 1 TO 6 WITH $\alpha = 0.9$

	Mode 1		Mode 2	
	$d(0,0,0.9)$	θ_{coh}	$d(0,0,0.9)$	θ_{coh}
Case 1	0.31 m	17.2°	0.28 m	22.9°
Case 2	0.25 m	17.2°	0.28 m	22.9°
Case 3	0.58 m	17.2°	0.66 m	22.9°
Case 4	0.16 m	22.9°	0.15 m	22.9°
Case 5	0.14 m	17.2°	0.15 m	22.9°
Case 6	0.9 m	22.9°	0.9 m	28.6°

TABLE II
AVERAGE COHERENCE DISTANCE AND COHERENCE POLAR ANGLE FOR CASE 7 AND 8 WITH $\alpha = 0.9$

	Mode 1		Mode 2	
	$\bar{d}(0,0,0.9)$	θ_{coh}	$\bar{d}(0,0,0.9)$	θ_{coh}
Case 7	0.34 m	11.4°	0.33 m	11.4°
Case 8	0.49 m	28.6°	0.49 m	28.6°

TABLE III
AVERAGE COHERENCE DISTANCE AND COHERENCE POLAR ANGLE FOR DIFFERENT $\Phi_{1/2}$ AND FOV, WITH θ AT MODE 1 AND $\alpha = 0.9$

	$\Phi_{1/2} = 30°$		$\Phi_{1/2} = 60°$	
	$\bar{d}(0,0,0.9)$	θ_{coh}	$\bar{d}(0,0,0.9)$	θ_{coh}
FOV=80°	0.49 m	28.6°	0.60 m	22.9°
FOV=60°	0.47 m	22.9°	0.51 m	17.2°
FOV=30°	0.20 m	5.7°	0.24 m	5.7°

denoted as θ_{coh}; 3) the minimum value of $\Delta\psi$ that satisfies $d(\boldsymbol{n}, 0, \Delta\psi, \alpha) = 0$ or $\bar{d}(0, \Delta\psi, \alpha) = 0$, named as coherence azimuthal angle. Since the VLC channel gain is fairly tolerant to the changes of azimuthal angle ψ[1], we mainly discuss the (average) coherence distance $d(\boldsymbol{n}, 0, 0, \alpha)$ and $\bar{d}(0, 0, \alpha)$, and the coherence polar angle in this section.

Given $\alpha = 0.9$, Table I lists the coherence distance $d(\boldsymbol{n}, 0, 0, \alpha)$ and coherence polar angle for Cases 1-6 with FOV $= 80°$ and $\Psi_{1/2} = 30°$. Firstly, by comparing Case 1 and Case 4 with Case 3 and Case 6, it can be seen that the coherence distance when a user is moving away or towards the LED is smaller than the coherence distance when the user's movement direction is nearly perpendicular to the line segment from the LED to the user. Since the VLC channel gain is a decreasing function of the relative distance between the LED and receiver, when a user moves in the direction $\boldsymbol{n}_1$ in the area B or area C, the relative distance between the LED and receiver increases rapidly, with the channel gain also rapidly decreasing. On the contrary, if the user moves in the direction $\boldsymbol{n}_3$, which is nearly perpendicular to the line segment from the LED to the receiver in the area B or area C, the distance between the LED and receiver varies slower, resulting into slower changes in the VLC channel gain. Secondly, if the receiver is inclined as in mode 1, the coherence distance when the user is moving away from the LED is different from that when the user is moving toward the LED. When a user is moving away from the LED, the receiver faces the LED, resulting in a smaller angle of incidence and more stable VLC channel gain. Therefore, the coherence distance when the user moving away from the LED (Case 1 and Case 4) is larger than that when the user moving toward the LED (Case 2 and Case 5). However, when the receiver orientation is almost vertical as in mode 2, Case 1 and Case 4 are equivalent to Case 2 and Case 5. Besides, it is shown that the coherence polar angle for mode 2 is a little larger than mode 1 for all cases, since the VLC channel becomes more sensitive to rotations when the receiver is already tilted.

Table II compares the average coherence distance $\bar{d}(0, 0, \alpha)$ and coherence polar angle for Cases 7 and 8 with $\alpha = 0.9$, FOV $= 80°$ and $\Psi_{1/2} = 30°$. Since VLC channel gains become more sensitive to receiver movements and rotations when the user is close to the LED, the average coherence distance and coherence polar angle decrease when user trajectories are limited to the center area A. In addition, we can see that mode 1 and mode 2 have a similar average performance, although there might be differences on some specific user trajectories.

Table III presents the average coherence distance $\bar{d}(0, 0, \alpha)$ and coherence polar angle for Case 8 with different $\Phi_{1/2}$ and FOV when polar angle θ is at mode 1 and $\alpha = 0.9$. As the receiver's FOV narrows, the received VLC channel gain could change greatly even with slight receiver movements and rotations. Therefore, the average coherence distance and coherence polar angle will be decreased. Meanwhile, since a wide emitting light beam generates more even illumination in a space than a narrow emitting light beam, the coherence distance when $\Phi_{1/2} = 60°$ is greater than that when $\Phi_{1/2} = 30°$.

The (average) coherence distance and coherence polar angle vary with different shapes of LED light beams, different FOV of receivers, as well as different types of user trajectories. However, most of the time, the (average) coherence distance with $\alpha = 0.9$ is several tens of centimeters and coherence polar angle is about 10-20 degrees. In other words, the VLC channel gain would remain relatively static if the receiver movement is within several tens of centimeters and the receiver rotation is less than 10 degrees. In addition, it can be concluded from Tables I to III that FOV and receiver movement patterns are two main influential factors to VLC channel variations. Since user trajectories are usually uncontrollable, an effective way to change channel variation characteristics is to change the receivers' FOV.

Besides, in multiple-input-multiple-output (MIMO) systems where a user is equipped with multiple PD receivers, those PDs for one user should have differentiable channel gains in order to obtain spatial multiplexing gain. Therefore, according to the analysis of coherence distance above, the spacing between those PDs should be at least several tens of centimeters. The spacing can be reduced if a lens is utilized to separate light from different directions. In this way, the effective FOV for each PD in the PD array is actually narrowed, and thus, the average coherence distance can be reduced. On the other hand, the spacing can also be reduced by adopting PDs with different orientations. Since coherence polar angle with $\alpha = 0.9$ is around 10-20 degrees, it is recommended that the difference between PD inclinations is in the order of 10 degrees.

[1]The coherence azimuthal angle is more than 90 degrees most of the time.

$$C_t(\tau) = E\{(h_t - \bar{h})(h_{t+\tau} - \bar{h})\} = E\{(h(\boldsymbol{R}_t, \theta_t, \psi_t) - \bar{h})(h(\boldsymbol{R}_{t+\tau}, \theta_{t+\tau}, \psi_{t+\tau}) - \bar{h})\} \quad (10)$$
$$\simeq E\{(h(\boldsymbol{R}_t, \theta_t, \psi_t) - \bar{h})(h(\boldsymbol{R}_t + v\tau\boldsymbol{n}, \theta_t + \Delta\theta_\tau, \psi_t + \Delta\psi_\tau) - \bar{h})\}$$
$$= E_{\boldsymbol{n},\Delta\theta_\tau,\Delta\psi_\tau}\{C(v\tau\boldsymbol{n}, \Delta\theta_\tau, \Delta\psi_\tau)\}$$

V. Correlation Function of VLC Channel Gain in The Time Domain

For a mobile user, the receiver location and orientation change with time, which leads to temporal VLC channel variations. The rate of VLC channel variations can be evaluated by the correlation function of VLC channel gain in the time domain. To calculate the correlation function of the VLC channel gain in the time domain, uniformly sampled user trajectories are usually required [11]. In order to capture VLC channel variations in various situations precisely, such as under different user velocities, the sampling rate of user trajectories has to be high. However, this leads to redundant data collection in scenarios where users move slow. If collected user trajectories have different sampling rates, extra data processing has to be performed [11]. To utilize user trajectories sampled with different rates more easily and to evaluate temporal VLC channel variations with only statistical information on receiver movements and rotations over time, we have the following assumptions,

- A user moves with constant velocity in a short period of time. Therefore, user trajectories can be approximated by connected line segments.
- The polar angle θ keeps constant within the coherence time of θ, while θ at time $t+\tau$ is independent of θ at time t if the time lag τ is larger than the coherence time[2].
- The azimuthal angle ψ is invariant when the user moves along a line segment in the user trajectory. The receiver's azimuthal angle takes independent values when the receiver is at different line segments. The changes of azimuthal angle ψ are independent of the changes of θ.

The correlation function of h in the time domain is defined by [14]

$$C_t(\tau) \triangleq E\{(h_t - \bar{h})(h_{t+\tau} - \bar{h})\} \quad (9)$$

where h_t denotes the VLC channel gain at time t.

Based on the above assumptions, the correlation function of VLC channel h in the time domain can actually be approximated by the MR correlation function as formulated in (10) at the top of the this page, where $\boldsymbol{R}_t, \theta_t, \psi_t$ denote the location, polar angle and azimuth angle of the receiver at time t. The user velocity is denoted as v. In addition, $\Delta\theta_\tau$ and $\Delta\psi_\tau$ denote the changes of θ and ψ after a time lag τ, respectively. It is worth noting that the joint PDF of receiver location and orientation is calculated as shown in (8) for the MR correlation function, which can deal with user trajectories using different sampling rates.

[2]The coherence time of θ refers to the time lag τ that leads to the correlation function of polar angle θ being 0, as discussed in [11].

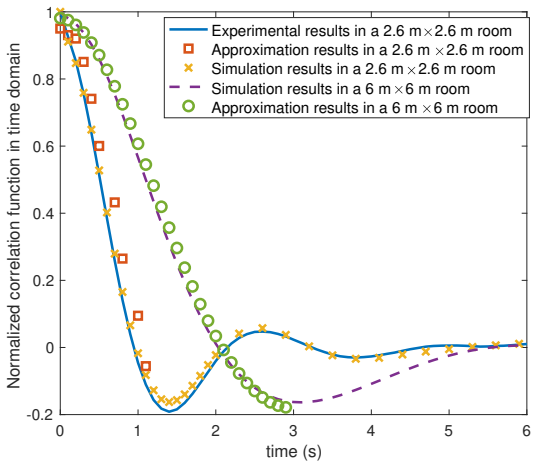

Fig. 11. The comparison between the normalized correlation function of the VLC channel gain in the time domain and its approximation based on MR correlation function.

According to assumption 2, the PDF of $\Delta\theta_\tau$ is given by

$$f(\Delta\theta_\tau) = \begin{cases} \delta(\Delta\theta_\tau) & \tau < \tau_a \\ \int_{-\infty}^{\infty} f(\theta) f(\theta + \Delta\theta_\tau)\, d\theta & \tau \geq \tau_a \end{cases} \quad (11)$$

where τ_a denotes the coherence time of θ discussed in [11] and $f(\theta)$ denotes the PDF of θ. $\delta(\cdot)$ is the Dirac function. The PDF of $\Delta\psi_\tau$ can be approximated by

$$f(\Delta\psi_\tau) = (1 - \frac{\tau v}{L})\delta(\Delta\psi_\tau) + \frac{\tau v}{L}\int_{-\infty}^{\infty} f(\psi) f(\psi + \Delta\psi_\tau)\, d\psi \quad (12)$$

where L denotes the average length of a line segment on the user trajectory and $f(\psi)$ is the PDF of ψ. The explanation of (12) is in the Appendix. In addition, the unit vector representing the receiver movement direction, i.e., $\boldsymbol{n}$, is assumed to be uniformly distributed in the horizontal user plane, namely that the azimuthal angle of $\boldsymbol{n}$ is uniformly distributed in [0,2π], and is independent of $\Delta\theta_\tau$ and $\Delta\psi_\tau$.

Essentially, via (10)–(12), the correlation function of the VLC channel gain in the time domain can be approximated by the MR correlation function using only the statistical distribution of the receiver movements and rotations. The coherence time of the VLC channel gain with the threshold of α can then be calculated accordingly, which is given by

$$\tau(\alpha) = \min\left\{\tau \in R^+ : \frac{C_t(\tau)}{C_t(0)} \leq \alpha\right\} \quad (13)$$

Figure 11 compares the normalized correlation function of the VLC channel gain in the time domain, namely $C_t(\tau)$ in (9) divided by $C_t(0)$, and its approximation via (10). The LED is at the center of the room, 2.31 m higher than the user

plane, and the ORWP mobility model is utilized to simulate the user trajectories, assuming v =1m/s, $\theta_0 = 28°$, and $\sigma = 7.8°$ [8]. Regarding the experimental result in Fig. 11, h_t is obtained by inquiring the channel gain at each point on the user trajectory from the experiments in Section III and then the correlation function of h_t in the time domain is computed by (9). Whereas, for the simulation results in Fig. 11, the channel gain at each point on the trajectory is simulated using the channel model in [4] with the identical parameters to the experiments. The approximation by MR correlation function is calculated as in (10). In particular, to compute the MR correlation function, the channel gains $h(\boldsymbol{R}, \theta, \psi)$ are simulated using [4] and the conditional PDF of receiver location and orientation is calculated by (8) according to history user trajectories. The history user trajectories are not identical to the user trajectory used to calculated h_t but they are simulated by the ORWP model with the same parameters. It is shown that the approximated correlation function of h_t in the time domain closely matches with the simulated and experimental results. Therefore, the MR correlation function is capable of approximating channel variations over time well, although only the statistical information about receiver location and orientation instead of the actual user trajectories are known. In addition, it can be seen from Fig. 11 that the coherence time when the user trajectory is limited to a small center area is shorter than that when the user moves in a wide space, which aligns with the results about coherence distance in Table II.

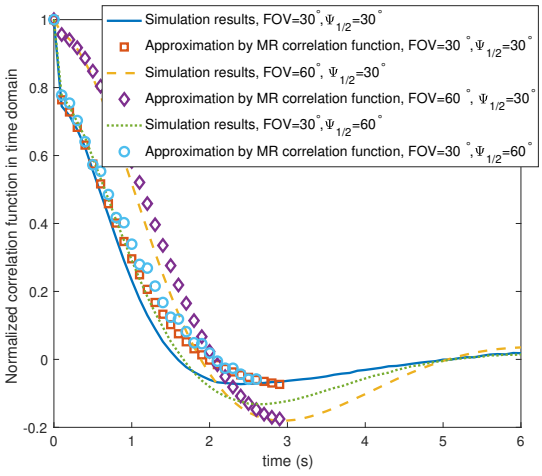

Fig. 12. The normalized correlation function of the VLC channel gain in the time domain with different FOV and $\Psi_{1/2}$.

Figure 12 illustrates the normalized correlation function of h_t in the 6 m $\times$ 6 m room specified in Section IV with different FOV and $\Psi_{1/2}$. The ORWP mobility model is utilized to simulate user trajectories, assuming v =1m/s, $\theta_0 = 28°$, and $\sigma = 7.8°$. Similar to the results about coherence distance in Section IV, the FOV of receiver is more influential on VLC channel variations. In addition, it can be seen that the difference between the approximation of $C_t(\tau)$ by the MR correlation function and the simulation result of $C_t(\tau)$ increases a bit when time τ increases. This is because the assumption, that a user moves with a constant velocity at a fixed direction, is not very accurate in the long term. Therefore, the approximation of $C_t(\tau)$ could deviate from the simulation result when τ becomes large. Especially when the FOV of receiver is very narrow, the VLC channel gain changes more sharply with the receiver movements and rotations. In this case, the inaccurate assumption of receiver movements could lead to the increased approximation error, as shown in Fig. 12. However, even when the FOV of receiver is narrow, the approximation of $C_t(\tau)$ by the MR correlation function matches well with the simulation result before the normalized $C_t(\tau)$ decreases to 0.2.

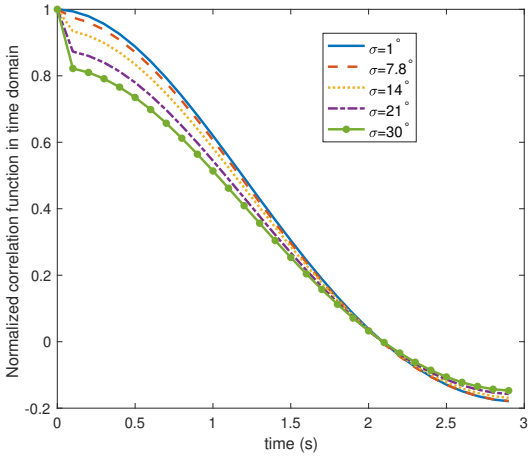

Fig. 13. The approximated correlation function of h_t in the time domain after normalization with different standard deviation of the polar angle.

Figure 13 shows the approximation of the normalized correlation function of h_t in the time domain as shown in (10) with different standard deviation of θ in the 6 m $\times$ 6 m room. The room layout is illustrated in Section IV and the ORWP mobility model is utilized to simulate user trajectories, assuming v =1m/s, $\theta_0 = 28°$, and $\sigma = 7.8°$. The changes of receiver orientation could be much faster than the receiver movement for low-speed mobile users. Therefore, when the standard deviation of receiver polar angle is intensified, the normalized channel correlation of the VLC channel gain in the time domain will quickly drop to a level smaller than 0.9 due to the effect of receiver rotations. Then, the decrease of C_t slows down. This is for the reason that receiver rotation usually leads to small fluctuations of the VLC channel gain, and to get relatively low channel correlation needs the accumulation of receiver movements, which is in accordance with the discussion about average coherence distance in Fig. 8.

VI. The Analysis of Spectral Efficiency Variations

As discussed in previous sections, the MR correlation function evaluates the VLC channel variation caused by the receiver movement and rotation. Moreover, the MR correlation function is able to approximate the correlation function of the VLC channel gain in the time domain. Accordingly, the coherence time, during which the VLC channel keeps relatively static, can be estimated.

Therefore, an important application of the MR correlation function is to help design the length and structure of data

transmission frames, aiming to ensure the stability of system performance and at the same time improve the efficiency of CSI feedback. Intuitively, when the estimated coherence time of the VLC channel is long, CSI update rate can be reduced. On the contrary, when the estimated coherence time is short, such as when users are moving in high-speed, CSI should be fed back more frequently to ensure robust system performance under varying VLC channels. However, how to choose a coherence time with a proper α as the criterion for CSI feedback and transmission adaptation still needs to be investigated.

In order to illustrate the relationship between system performance and MR correlation function more specifically, we take a single-input-single-output (SISO) VLC system as an example. In the SISO VLC system, the user estimates the instantaneous CSI based on received signals and then feeds the CSI back to the transmitter, which is repeated each period of T for adaptive data transmission. Since the VLC channel is relatively stable within the coherence time, it is sensible to set the CSI feedback period T as the coherence time $\tau(\alpha)$ with a threshold α. The coherence time $\tau(\alpha)$ can be calculated according to the MR correlation function as shown in (13). Afterwards, the transmitter can adapt the transmitting power based on the CSI feedback to achieve a required spectral efficiency. Specifically, the transmitting power P during the k-th CSI feedback period is adjusted to satisfy the following equation

$$\log_2(1+\frac{P|h_{kT}|^2}{\sigma^2}) = R_{\rm th} \tag{14}$$

where $R_{\rm th}$ denotes the expected spectral efficiency, σ^2 is the noise power and h_{kT} refers to the CSI fed back at the kth period. More specifically, h_{kT} is the instantaneous channel gain estimated at time kT, the start of the k-th CSI feedback period. Due to the variations of the VLC channel, h_{kT} is not exactly the same as the channel after a time lag $\tau < T$. Hence, the true spectral efficiency at the time $kT+\tau$ is given by

$$\begin{aligned} R &= \log_2(1+\frac{P|h_{kT+\tau}|^2}{\sigma^2}) = \log_2(1+\frac{P|h_{kT}+\Delta h|^2}{\sigma^2}) \\ &= R_{\rm th} + \frac{2\log_2(e)P\hat{h}/\sigma^2}{1+P|\hat{h}|^2/\sigma^2}\Delta h \\ &= R_{\rm th} + \frac{2\log_2(e)P|\hat{h}|^2/\sigma^2}{1+P|\hat{h}|^2/\sigma^2}\frac{\Delta h}{\hat{h}} \end{aligned} \tag{15}$$

where $\hat{h}$ is a value between h_{kT} and $h_{kT+\tau}$ according to the Lagrange's Mean Value Theorem. Therefore, the average difference between the true spectral efficiency and $R_{\rm th}$ can be formulated as

$$\begin{aligned} &E\{|R-R_{\rm th}|\} = E\{\frac{2\log_2(e)P|\hat{h}|^2/\sigma^2}{1+P|\hat{h}|^2/\sigma^2}\frac{|\Delta h|}{\hat{h}}\} \\ \le& E\{2\log_2(e)\frac{|h_{kT+\tau}-h_{kT}|}{\hat{h}}\} \end{aligned} \tag{16}$$

where $E\{\cdot\}$ means the expectation operation. Moreover, since the signal-to-noise ratio (SNR) for users in a VLC system is usually larger than 1 [19], [20], (16) can be rewritten as

$$\begin{aligned} &E\{|R-R_{\rm th}|\} = E\{\frac{2\log_2(e)P|\hat{h}|^2/\sigma^2}{1+P|\hat{h}|^2/\sigma^2}\frac{|\Delta h|}{\hat{h}}\} \\ \simeq& E\{2\log_2(e)\frac{|h_{kT+\tau}-h_{kT}|}{\hat{h}}\} \end{aligned} \tag{17}$$

The average spectral efficiency fluctuation compared with $R_{\rm th}$ in a CSI feedback period can then be bounded by

$$\begin{aligned} &E\{|R-R_{\rm th}|\} \\ &\overset{(a)}{\le} 2\log_2(e)\sqrt{E\{(h_{kT+\tau}-h_{kT})^2\}E\{\frac{1}{\hat{h}^2}\}} \\ =&2\log_2(e)\sqrt{2\frac{E\{(h_{kT}-\bar{h})^2-(h_{kT+\tau}-\bar{h})(h_{kT}-\bar{h})\}}{E\{(h_{kT}-\bar{h})^2\}}} \\ &\times\sqrt{E\{(h_{kT}-\bar{h})^2\}E\{\frac{1}{\hat{h}^2}\}} \\ \simeq& 2\log_2(e)\sqrt{2C_t(0)E\{\frac{1}{h_{kT}^2}\}}\sqrt{1-\frac{C_t(\tau)}{C_t(0)}} \\ &\overset{(b)}{\le} 2\log_2(e)\sqrt{2C_t(0)E\{\frac{1}{h_{kT}^2}\}}\sqrt{1-\alpha} \triangleq e(\alpha) \end{aligned} \tag{18}$$

where (a) holds due to the Cauchy-Bunyakovsky-Schwarz inequality. In the fourth line, $E\{\frac{1}{\hat{h}^2}\}$ is approximated by $E\{\frac{1}{h_{kT}^2}\}$ based on the assumption that VLC channel variations are limited within the coherence time and thus the difference between h_{kT}, $h_{kT+\tau}$ and $\hat{h}$ should be small[3]. Meanwhile, (b) is derived according to the definition of coherence time in (13). As shown in (18), the difference between the true spectral efficiency and $R_{\rm th}$ is limited by a square root function of $1-\alpha$, denoted as $e(\alpha)$. With a large α, the CSI feedback period $\tau(\alpha)$ is short, leading to small spectral efficiency variations but high feedback overhead. On the contrary, choosing a CSI feedback period corresponding to a small α could reduce the feedback overhead at the expense of large spectral efficiency fluctuations. Therefore, given the upper bound function $e(\alpha)$ of spectral efficiency fluctuations, the system could determine a proper α to realize a tradeoff between spectral efficiency fluctuations and the cost of CSI feedback.

Figure 14 illustrates the average spectral efficiency fluctuation, namely, $E\{|R-R_{\rm th}|\}$, with different α for the CSI feedback period $\tau(\alpha)$. To compute $E\{|R-R_{\rm th}|\}$ and its upper bound $e(\alpha)$, h_t is simulated according to the ORWP model and C_t is approximated by the MR correlation function as in Section V, assuming $v = 1$ m/s, $\theta_0 = 28°$, $\sigma = 7.8°$ and FOV $= 80°$. The average spectral efficiency fluctuation approaches 0 when $\alpha \simeq 1$, because, in this case, $\tau(\alpha)$ is extremely small and the transmitter could get the newest CSI. As α decreases, $\tau(\alpha)$ becomes longer and the accuracy of CSI feedback will be degraded, which aggravates the instability of the achievable spectral efficiency accordingly. The upper

[3]To avoid $\frac{1}{h^2}$ getting impractically large due to some extremely small values of h, we compute $E\{\frac{1}{h^2+\varsigma}\}$ instead, where ς is a relatively small number compared to the average channel gain.

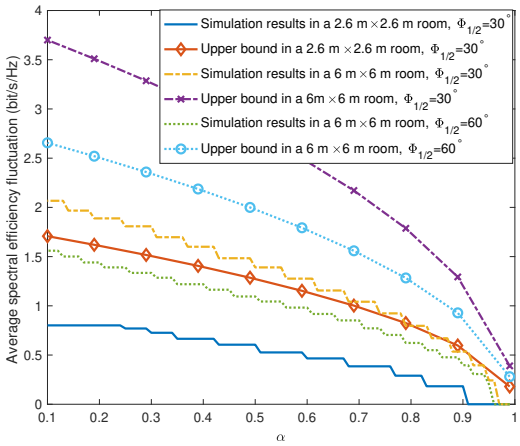

Fig. 14. The average fluctuation of spectral efficiency from $R_{\rm th}$ with different α for CSI feedback period $\tau(\alpha)$.

bound $e(\alpha)$ could give a rough depiction of the relationship between α and $E\{|R - R_{\rm th}|\}$ using a simple expression. Moreover, it is fairly safe to determine α and CSI feedback period $\tau(\alpha)$ based on $e(\alpha)$, since the actual spectral efficiency fluctuation will be smaller than that indicated by the upper bound. For instance, in Fig. 14, the upper bound $e(\alpha)$ is about 2 times larger than the actual spectral efficiency fluctuation. In addition, it is shown that the fluctuation of spectral efficiency is also related to the factor $\sqrt{2C_t(0)E\{\frac{1}{h^2}\}}$. If the LED illumination is uneven, such as when the emitting light beam is narrow or the room is relatively spacious, $\sqrt{2C_t(0)E\{\frac{1}{h^2}\}}$, particularly $E\{\frac{1}{h^2}\}$, is big, which indicates the quick growth of the spectral efficiency fluctuation with the decrease of α. Therefore, the proper α for different scenarios should be decided adaptively based on $e(\alpha)$.

VII. Conclusions and Future Work

In this paper, the MR correlation function is proposed as a useful tool to evaluate VLC channel variations due to receiver movements and rotations. Moreover, the correlation function of the VLC channel gain in the time domain and the coherence time can also be approximated by the MR correlation function to measure channel variations over time, which facilitates determining data transmission frames and CSI feedback frequency. Various parameters that influence the MR correlation function have been studied via simulations and experiments, where receiver's FOV is an influential factor. Meanwhile, it is found that a receiver movement of several tens of centimeters or a change of 10-20 degrees in the inclined angle of the receiver is required in a typical scenario in order to observe a distinguishable change of VLC channel gain.

In the future work, we would like to investigate the extensions of the MR correlation function, to evaluate channel variations in more complicated scenarios. Several future research directions are listed

1) Extend the definition of MR correlation function to multiple-LED scenarios. The MR correlation function evaluates the variations of the VLC channel between an LED and a PD. When there are multiple LEDs, how the VLC channel gain vector between one PD and multiple LEDs changes should be investigated.

2) Extend the definition of MR correlation function to investigate the effects of vertical receiver movements on the VLC channel variations. In this paper, only the horizontal receiver movements are considered. Actually, the receiver movement could include both vertical and horizontal components. These two components could have different probabilities of occurrence and different ranges of variations. How the VLC channel gain changes under vertical and horizontal receiver movements, as well as receiver rotations, should be investigated.

3) Extend the definition of MR correlation function in order to measure the stability of the link between a PD and an LED. When the FOV of the receiver or the emitting light beam is extremely narrow, the VLC channel gains within the coverage of an LED are fairly even but the coverage itself is small, leading to high outage probability. In this case, the changes of PD-LED link availability, besides the actual changes of VLC channel gain, should be investigated.

Appendix

A. Explanation of (12)

According to the assumption of receiver movements and rotations in Section V, the trajectories of a receiver can be approximated by connected line segments. On each line segment, the azimuthal angle ψ can be assumed constant. Therefore, supposing the length of a line segment is l and user velocity as v, there is a probability of $1 - \frac{\tau v}{l}$ that the receiver will move on this line segment for at least a duration of τ. In this situation, $\Delta\psi_\tau = 0$. The probability that the receiver is at the end part of this segment and will turn to next line segment within the duration τ is $\frac{\tau v}{l}$. In this case, $\Delta\psi_\tau = \psi_2 - \psi_1$, where ψ_1 is the current azimuthal angle and ψ_2 is the value of the azimuthal angle on the next line segment. According to the assumption in Section V, ψ_2 and ψ_1 are independent and identically distributed random variable with PDF as $f(\psi)$. Therefore, the PDF of their difference $\Delta\psi_\tau$ is equal to $\int_{-\infty}^{\infty} f(\psi)f(\psi + \Delta\psi_\tau)\,d\psi$. Replacing l by the average length of a line segment L, the PDF of $\Delta\psi_\tau$ can be approximated by (12).

References

[1] M. Obeed, A. M. Salhab, M.-S. Alouini, and S. A. Zummo, "On optimizing VLC networks for downlink multi-user transmission: A survey," *IEEE Communications Surveys & Tutorials,* vol. 21, no. 3, pp. 2947–2978, 3rd Quarter 2019.

[2] A.-M. Cailean, and M. Dimian, "Current challenges for visible light communications usage in vehicle applications: A survey," *IEEE Communications Survey & Tutorials,* vol. 19, no. 4, pp. 2681–2703, 4th Quarter 2017.

[3] H. Schulze, "Frequency-domain simulation of the indoor wireless optical communication channel," *IEEE Transactions on Communications,* vol. 64, no. 6, pp. 2551–2562, Jun. 2016.

[4] K. Lee, H. Park, and J. R. Barry, "Indoor channel characteristics for visible light communications," *IEEE Communications Letters,* vol. 15, no. 2, pp. 217–219, Feb. 2011.

[5] A. Al-Kinani, J. Sun, C. Wang, W. Zhang, X. Ge, and H. Haas, "A 2-D non-stationary GBSM for vehicular visible light communication channels," *IEEE Transactions on Wireless Communications,* vol. 17, no. 12, pp. 7981–7992, Dec. 2018.

[6] B. Turan, G. Gurbilek, A. Uyrus, and S. C. Ergen, "Vehicular VLC frequency domain channel sounding and characterization," in Proc. *2018 IEEE Vehicular Networking Conference (VNC),* Dec. 5–7, 2018.
[7] M. Jani, P. Garg and A. Gupta, "Performance analysis of a mixed cooperative PLC-VLC system for indoor communication systems," to appear in *IEEE Systems Journal,* 2019.
[8] M. D. Soltani, A. A. Purwita, Z. Zeng, H. Haas, and M. Safari, "Modeling the random orientation of mobile devices: measurement, analysis and LiFi use case," *IEEE Transactions on Communications,* vol. 67, no. 3, 2157–2172, Mar. 2019.
[9] M. D. Soltani, X. Wu, M. Safari, and H. Haas, "Bidirectional user throughput maximization based on feedback reduction in LiFi networks," *IEEE Transactions on Communications,* vol. 66, no. 7, pp. 3172–3186, Jul. 2018.
[10] S. Feng, R. Zhang, X. Li, Q. Wang, and L. Hanzo, "Dynamic throughput maximization for the user-centric visible light downlink in the face of practical consideration," *IEEE Transactions on Wireless Communications,* vol. 17, no. 8, pp. 5001–5015, Aug. 2018.
[11] A. A. Purwita, M. D. Soltani, M. Safari, and H. Haas, "Terminal orientation in OFDM-based LiFi systems," *IEEE Transactions on Wireless Communications,* vol. 18, no. 8, pp. 4003–4016, Aug. 2019.
[12] M. D. Soltani, Z. Zeng, H. Kazemi, C. Chen, H. Haas, M. Safari, "A study of sojourn time for indoor LiFi cellular networks," in Proc. *2019 IEEE 30th Annual International Symposium on Personal, Indoor and Mobile Radio Communications (PIMRC),* Sep. 8–11, 2019.
[13] D. Bykhovsky, "Coherence distance in indoor optical wireless communication channels," *Optics Letters,* vol. 43, no. 10, pp. 2248–2251, May 2018.
[14] T. S. Rappaport, Wireless Communications: Principles and Practice. IEEE Press, 1996.
[15] B. Sklar, "Rayleigh fading channels in mobile digital communication systems. I. characterization," *IEEE Communications Magazine,* vol. 35, pp. 136–146, Sep. 1997.
[16] U. Schilcher, J. F. Schmidt, M. K. Atiq, and C. Bettstetter, "Autocorrelation and coherence time of interference in Poisson Networks," to appear in *IEEE Transactions on Mobile Computing,* 2019.
[17] C. Bettstetter and C. Wagner, "The spatial node distribution of the random waypoint mobility model," In *Proc. German Workshop on Mobile Ad Hoc Networks (WMAN)*, Ulm, Germany, Mar. 2002.
[18] M. Kashef, M. Ismail, M. Abdallah, K. A. Qaraqe, and E. Serpedin, "Energy efficiency resource allocation for mixed RF/VLC heterogeneous wireless networks," *IEEE Journal on Selected Areas in Communications*, vol. 34, no. 4, pp. 883–893, Apr. 2016.
[19] M. A. Arfaoui, M. D. Soltani, I. Tavakkolnia, A. Ghrayeb, C. Assi, H. Haas, and M. Safari, "SNR statistics of indoor mobile VLC users with random device orientation," in *Proc. 2019 IEEE International Conference on Communications Workshops (ICC Workshops)*, Shanghai, China, May 2019.
[20] M. Rahaim and T. D. C. Little, "Interference in IM/DD optical wireless communication networks," *IEEE/OSA Journal of Optical Communnications and Networking*, vol. 9, no. 9, pp. D51–D63, Sep. 2017.
[21] X. Li, F. Jin, R. Zhang, J. Wang, Z. Xu, and L. Hanzo, "Users first: user-centric cluster formation for interference-mitigation in visible-light networks," *IEEE Transactions on Wireless Communications*, vol. 15, no. 1, pp. 39–53, Jan. 2016.

Jiaxuan Chen received her B.S. degree from Tsinghua University in 2016, where she is currently working toward the Ph.D. degree with the Department of Electronic Engineering, Tsinghua University.
Her current research interests include wireless communications, signal processing, optical wireless communications and vehicular ad-hoc networks.

Iman Tavakkolnia (S'15, M'19) received the B.Sc. degree in telecommunication engineering from the University of Tehran, Tehran, Iran, in 2006, the M.Sc. degree in communication systems from the Sharif University of Technology, Tehran, in 2011, and the Ph.D. degree in electrical engineering from The University of Edinburgh, Edinburgh, U.K., in 2018, where he is currently a Research Associate with the LiFi Research and Development Centre. His research interests include communication theory, optical fiber communication, and visible light communication.

Cheng Chen (S'14) received the B.Eng. degree in electronic and electrical engineering from the University of Strathclyde, Glasgow, U.K., in 2011, the M.Sc. degree in communications and signal processing from the Imperial College, London, U.K., in 2012, and the Ph.D. degree in electrical engineering from the University of Edinburgh, Edinburgh, U.K., in 2017. He is currently employed as a Research Associate with the Li-Fi Research and Development Centre, The University of Edinburgh, where he is working in the field of visible light communications.

Zhaocheng Wang (M'09-SM'11) received his B.S., M.S. and Ph.D. degrees from Tsinghua University in 1991, 1993 and 1996, respectively. From 1996 to 1997, he was a Post-Doctoral Fellow with Nanyang Technological University, Singapore. From 1997 to 1999, he was a Research Engineer/Senior Engineer with OKI Techno Centre Pte. Ltd., Singapore. From 1999 to 2009, he was a Senior Engineer/Principal Engineer with Sony Deutschland GmbH, Germany. Since 2009, he has been a Professor with Department of Electronic Engineering, Tsinghua University, where he is currently the Director of Broadband Communication Key Laboratory, Beijing National Research Center for Information Science and Technology (BNRist).
His research interests include millimeter wave communications, Terahertz wireless communications and optical wireless communications. Prof. Wang hold 34 US/EU granted patents (23 of them as the first inventor) and published more than 150 peer-reviewed international journal papers. He authored or co-authored two books, which have been selected by IEEE Series on Digital & Mobile Communication and published by Wiley-IEEE Press.
Prof. Wang is a Fellow of the Institution of Engineering and Technology. He received ICC2013 Best Paper Award, OECC2015 Best Student Paper Award, 2016 IEEE Scott Helt Memorial Award, 2016 IET Premium Award, 2016 National Award for Science and Technology Progress (First Prize), ICC2017 Best Paper Award, and 2018 IEEE ComSoc Asia-Pacific Outstanding Paper Award. He is currently an Associate Editor of IEEE Transactions on Communications, an Associate Editor of IEEE Systems Journal, and an Associate Editor of IEEE Open Journal of Vehicular Technology. He was previously an Associate Editor of IEEE Transactions on Wireless Communications from 2011 to 2015 and an Associate Editor of IEEE Communications Letters from 2013 to 2016.

Harald Haas (S'98-AM'00-M'03-SM'16-F'17) received the Ph.D. degree from the University of Edinburgh in 2001. He currently holds the Chair of Mobile Communications at the University of Edinburgh, and is the Initiator, Co-Founder, and the Chief Scientific Officer of pureLiFi Ltd., and the Director of the LiFi Research and Development Center, the University of Edinburgh. He has authored 400 conference and journal papers, including a paper in Science and co-authored the book *Principles of LED Light Communications Towards Networked Li-Fi* (Cambridge University Press, 2015). His main research interests are in optical wireless communications, hybrid optical wireless and RF communications, spatial modulation, and interference coordination in wireless networks. He first introduced and coined spatial modulation and LiFi. LiFi was listed among the 50 best inventions in *TIME* Magazine 2011. He was an invited speaker at TED Global 2011, and his talk on "Wireless Data from Every Light Bulb" has been watched online over 2.4 million times. He gave a second TED Global lecture in 2015 on the use of solar cells as LiFi data detectors and energy harvesters. This has been viewed online over 1.8 million times. He was elected as a fellow of the Royal Society of Edinburgh in 2017. In 2012 and 2017, he was a recipient of the prestigious Established Career Fellowship from the Engineering and Physical Sciences Research Council (EPSRC) within Information and Communications Technology in the U.K. In 2014, he was selected by EPSRC as one of ten Recognising Inspirational Scientists and Engineers (RISE) Leaders in the U.K. He was a co-recipient of the EURASIP Best Paper Award for the *Journal on Wireless Communications and Networking* in 2015, and co-recipient of the Jack Neubauer Memorial Award of the IEEE Vehicular Technology Society. In 2016, he received the Outstanding Achievement Award from the International Solid State Lighting Alliance. He was a co-recipient of recent best paper awards at VTC-Fall, 2013, VTC-Spring 2015, ICC 2016, and ICC 2017. He is an Editor of the IEEE TRANSACTIONS ON COMMUNICATIONS and the IEEE JOURNAL OF LIGHTWAVE TECHNOLOGIES.